Integrative intratumoral and peritumoral radiomic model for predicting endometrial cancer grade

JIE REN[1], TINGTING CUI[1], XINGPENG LI[1], YANXIAO ZHANG[1], ZHIWEI SHEN[2] and YUNLONG YUE[1]

[1]Department of Medical Imaging, Beijing Shijitan Hospital, Capital Medical University, Beijing 100038, P.R. China; [2]Philips Healthcare, Beijing 100600, P.R. China

Received April 2, 2025; Accepted July 28, 2025

DOI: 10.3892/ol.2025.15228

Abstract. Non-invasive preoperative assessment of tumor grade serves an important role for clinical management. The aim of the present study was to assess the value of an intratumoral and an peritumoral radiomic model in predicting the histological grade of endometrial cancer (EC). A total of 107 patients with EC were retrospectively enrolled and randomly divided into the training (n=74) and test cohorts (n=33). Radiomic features were extracted from intratumoral and peritumoral regions (RT) with different expansion regions (1, 2 and 3 mm) using T2-weighted and the 5 to 8th phase of contrast-enhancement images. The diagnostic performance of several peritumoral features was compared with the maximum area under the curve (AUC) value. These intratumoral features were combined with peritumoral features to construct a fusion model. The AUCs for the RT model were 0.879 [95% confidence interval (CI), 0.797-0.962] for the training cohort and 0.869 (95% CI, 0.590-1.000) for the test cohort. The peritumoral model with a 3-mm expansion (RT-3) demonstrated superior performance, yielding AUCs of 0.934 (95% CI, 0.875-0.994) in the training cohort and 0.875 (95% CI, 0.744-1.000) in the test cohort. The fusion model incorporating features from both RT and RT-3 achieved the highest diagnostic performance for distinguishing low-grade from high-grade EC, with AUCs of 0.955 (95% CI, 0.910-1.000) and 0.885 (95% CI, 0.771-1.000) in the training and test cohorts, respectively. In conclusion, the results of the present study indicate that radiomic features from magnetic resonance images incorporating both intratumoral and peritumoral regions can effectively predict low-and high-grade EC.

Correspondence to: Professor Yunlong Yue, Department of Medical Imaging, Beijing Shijitan Hospital, Capital Medical University, 10 Yangfangdian Tieyiyuan Road, Haidian, Beijing 100038, P.R. China
E-mail: yueyunlong@bjsjth.cn

Abbreviations: EC, endometrial cancer; RT, endometrial cancer; LVSI, lymph vascular space invasion; ROI, region of interest; DCE, dynamic contrast-enhanced; FIGO, International Federation of Gynecology and Obstetrics; T2W1, T2-weighted imaging; mRMR, maximum relevance and minimum redundancy; LASSO, least absolute shrinkage and selection operator.

Key words: endometrial cancer, magnetic resonance imaging, radiomics

Introduction

Endometrial cancer (EC) is the most common malignancy of the female genital tract in developed countries (1). According to the International Agency for Research on Cancer, ~67,880 new cases and 13,250 mortalities have been reported globally due to EC in 2024 (2). Risk factors for EC include sustained estrogen exposure, metabolic abnormalities such as obesity and diabetes, and genetic susceptibility, such as Lynch syndrome and nulliparity (3). The histological subtype, pathological grade and stage of the tumor have been reported to markedly impact patient prognosis (4). According to the European Society of Gynecological Oncology, European Society for Radiotherapy and Oncology, European Society of Pathology and National Comprehensive Cancer Network guidelines, different grades and stages of EC require the corresponding management strategies. For example, patients with low-grade, stage IA endometrioid carcinoma typically do not require lymph node dissection or postoperative adjuvant radiotherapy, which leads to the reduction of unnecessary complications (4,5).

Currently, magnetic resonance imaging (MRI) exhibits a high specificity and accuracy in evaluating the depth of myometrial invasion, cervical stromal invasion and lymph node metastasis in EC, providing an important basis for preoperative non-invasive staging assessments (6-9). However, histological grading has traditionally relied on diagnostic dilation and curettage, which can be influenced by the sampling location and tumor volume, potentially causing discrepancies between preoperative and postoperative grades. In addition, this invasive procedure exhibits a potential risk of bleeding and infection, highlighting the need for non-invasive preoperative assessment of the tumor grade (9).

Radiomics, a novel quantitative analysis method, enables high-throughput feature extraction and model construction using extensive computation and decision-making logic. The workflow includes image acquisition, delineation of the region of interest (ROI), feature extraction and selection and model establishment. Radiomics has demonstrated a notable

role in disease diagnosis, treatment selection and prognosis prediction (10-15). Traditional MRI-based radiomic has previously been studied for predicting several aspects of EC, such as myometrial invasion, lymph node metastasis, lymph vascular space invasion and staging in EC (16-19). Several studies have investigated the distinction of the pathological grades of EC: Bonatti *et al* (20) reported that the ratio of tumor volume to uterine volume could differentiate between G1 and G2-G3 EC; Nougaret *et al* (21) reported that a tumor volume-to-uterine volume ratio of >25% was associated with G3 EC; the grading of EC using MR radiomics was investigated by Yue *et al* (22), reporting that EC grade could be predicted using radiomics score based on multiparametric MRI with area under the curve (AUC) of 0.837; and Zheng *et al* (23) demonstrated that a radiomics model combined with clinical indicators could increase the AUC value for pathological grading of EC to 0.925. However, previous studies that combined intratumoral and peritumoral radiomic features for predicting EC pathological grade are limited. Therefore, the present study aimed to assess the value of intratumoral and peritumoral radiomic features in predicting the histological grade of EC.

Materials and methods

Patients. The present retrospective study analyzed preoperative plain and dynamic contrast-enhanced (DCE) MR images from patients who were surgically treated for EC at Beijing Shijitan Hospital (Beijing, China) from January 2020 to May 2024. The present study was approved by the ethics committee of Beijing Shijitan Hospital [approval no. sjtkyll-lx-2020(3)] and written informed consent was obtained from all patients. All diagnoses were confirmed using surgical pathological assessment. The histological grading was based on the 2009 diagnostic criteria of the International Federation of Gynecology and Obstetrics (FIGO) (24): G1 and G2 were defined as low grade, and G3 as high grade. The inclusion criteria were as follows: i) No tumor-related treatment prior to MRI; ii) MRI examination performed within 30 days of surgery; iii) availability of complete postoperative pathological results; and iv) images free of notable artefacts within the volume of interest (VOI). If motion artifacts appeared only outside the uterus and did not affect the analysis and measurement of the tumor inside the uterus, the samples were still included. The exclusion criteria included the following: i) Tumors with a maximum diameter of <1 cm; ii) EC concurrent with other malignancies; and iii) image with excessive artefacts affecting VOI delineation. The patient selection flowchart is shown in Fig. 1.

MRI acquisition. A 1.5T MRI scanner (Ingenia; Philips Healthcare) and a 16-channel body phased array coil was utilized. The body coil was focused at the center of the pelvis and the scanning range included the area from the pubic symphysis to the upper abdomen. The scanning parameters were as follows: i) Axial and sagittal T2-weighted imaging (T2WI) turbo spin-echo sequences [repetition time (TR), 3,000 msec/2,500 msec; echo time (TE), 110/120 msec; echo train length, 20; field of view (FOV), 240x40 mm/250x278 mm; matrix, 268x253 m/280x308 m; slice thickness, 4 mm/6 mm; interslice gap, 0.4 mm/0.6 mm; number of excitations (NEX), 1]; ii) sagittal T1 mDIXION DCE sequences (TR, 5.8 msec, TE, 1.73 msec, FOV, 300x300 mm; matrix, 188x188 mm; slice thickness, 2.5 mm; interslice gap, -1.25 mm; NEX, 1). Following the intravenous injection of 0.2 mmol/kg of the contrast agent gadopentetate dimeglumine (gadopentetate dimeglumine injection, CONSUN), 25 dynamic scans were acquired. The duration of sagittal T2WI and DCE scanning was 2 min and 7 sec, and 2 min and 58 sec, respectively. Free breathing was used during all sequence scanning.

Tumor segmentation and radiomic feature extraction. DICOM images were exported from the image archiving and communication system and underwent pre-processing, including N4 bias field correction and Z score normalization and resampling to a voxel size of 1x1x1 mm. The pre-processed images were subsequently imported into ITK-snap software (version 4.2.0; https://www.itksnap.org/) for the image segmentation. A radiologist with 6 years pelvic imaging experience manually delineated the peritumoral regions (RT) on sagittal T2WI and early DCE images (5 to 8th phase) (25) using the extended functionality of 3D Slicer software (version 5.0.3; https://www.slicer.org/). The delineations were subsequently reviewed by two radiologists with >10 years experience in diagnosing gynecological tumors. The disagreements were resolved through consensus. The RT mask was subsequently expanded by 1 to 3 mm to generate peritumoral regions (RT-1, RT-2 and RT-3) with the expansion function of 3D Slicer software.

Using PyRadiomics (version 3.0.1; https://pyradiomics.readthedocs.io/en/latest/) on Python, 2,394 radiomic features were extracted from RT, RT-1, RT-2 and RT-3 on T2WI and Contrast-enhancement (CE)-T1WI. The features included geometric (volume, perimeter and maximum diameter), first-order (skewness, kurtosis, mean, root mean square and the median) and texture categorized into five types as follows: Grey-level co-occurrence matrix, grey-level run-length matrix, grey-level size zone matrix, grey-level dependence matrix and neighboring grey tone difference matrix. Each feature underwent Z score normalization. Radiomic features from T2WI and CE-T1WI were subsequently used for comprehensive analysis (Fig. 2).

Radiomics feature selection and model building. Feature selection involved the following key steps: i) Retaining features with $P<0.05$ using the Mann-Whitney U test or Student's t-test; ii) excluding highly correlated features (Pearson correlation coefficient, >0.9) to ensure non-redundancy; iii) the maximum relevance and minimum redundancy (mRMR) and least absolute shrinkage and selection operator (LASSO) methods were employed with the λ parameter optimized via 10-fold cross-validation. The optimal λ was subsequently used to calculate the coefficients of each feature and the features with nonzero coefficients were selected. These optimal features from RT, RT-1, RT-2 and RT-3, along with their non-zero coefficients were utilized to construct a logistic regression model. In addition, the best-performing intratumoral and peritumoral features were combined to predict the EC grade.

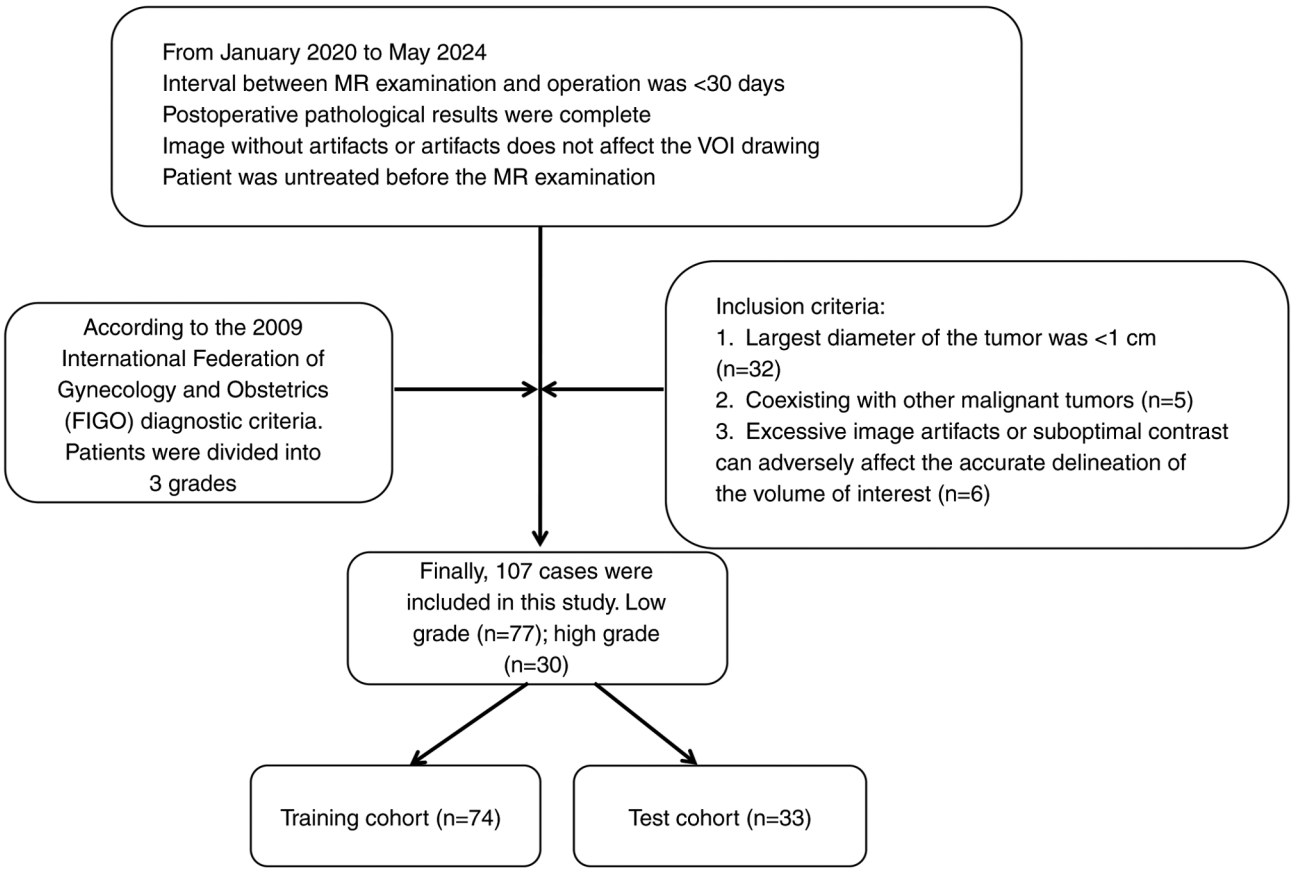

Figure 1. Patient recruitment and selection workflow. VOI, volume of interest.

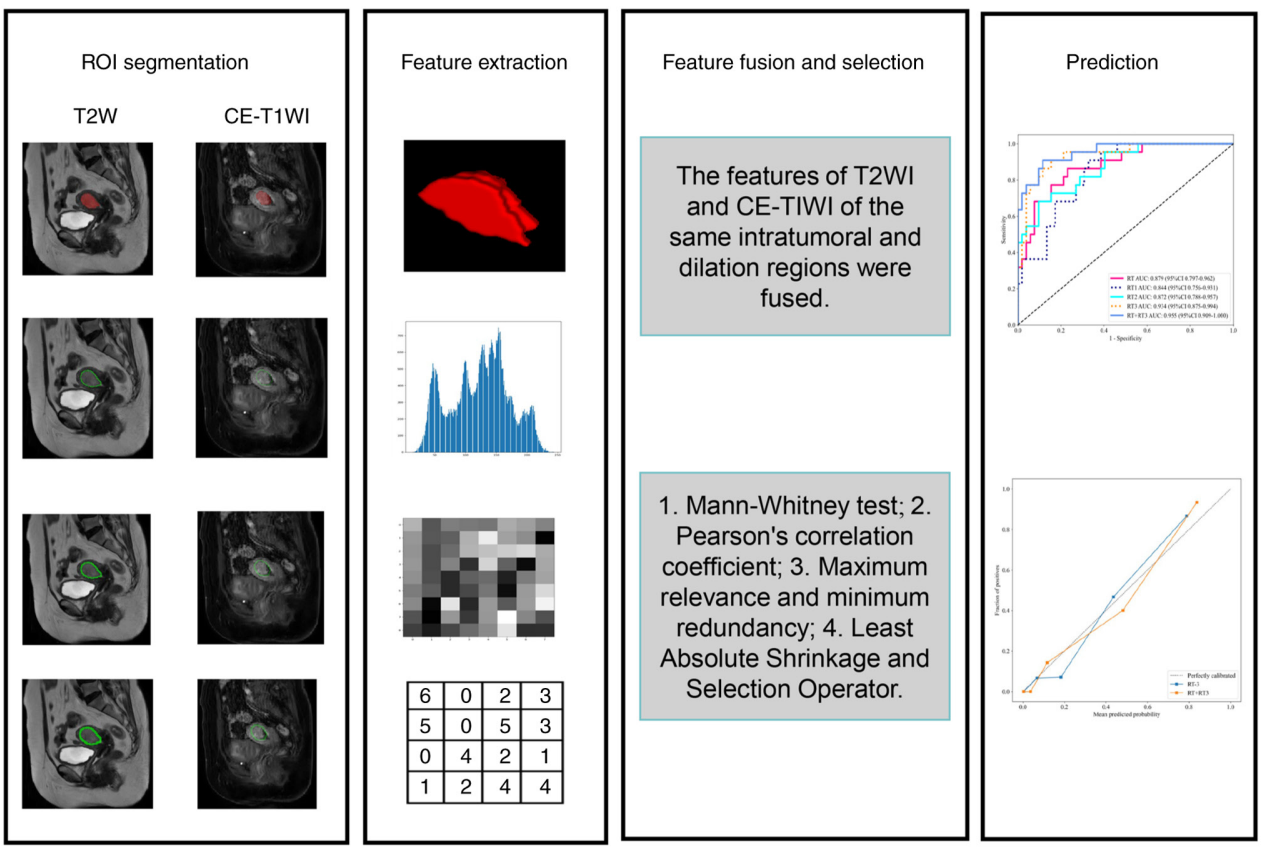

Figure 2. Steps in the workflow of the present study: Image acquisition, ROI delineation, feature extraction, feature selection, feature fusion and Rad signature building. ROI, region of interest; CE-T1WI, contrast enhancement T1-weighted imaging; AUC, area under curve; RT, peritumoral region.

Table I. Demographic and clinical characteristics of the patients.

	Training cohort (n=74)			Testing cohort (n=33)		
Characteristic	Low-grade (n=52)	High-grade (n=22)	P-value	Low-grade (n=25)	High-grade (n=8)	P-value
Age, years	55.50±10.65	58.55±8.81	0.245	56.92±12.25	53.38±10.31	0.400
Family history			>0.999			0.560
No	48 (92.31)	20 (90.91)		22 (88.00)	8 (100.00)	
Yes	4 (7.69)	2 (9.09)		3 (12.00)	0	
Myometrial invasion			0.380			0.366
<50%	41 (78.85)	15 (68.18)		20 (80.00)	5 (62.50)	
>50%	11 (21.15)	7 (31.82)		5 (20.00)	3 (37.50)	
FIGO stage			0.049			>0.999
I	46 (88.46)	15 (68.18)		23 (92.00)	7 (87.50)	
II-IV	6 (11.54)	7 (31.82)		2 (8.00)	1 (12.50)	
Lymph node status			0.060			0.242
Negative	50 (96.15)	18 (81.82)		25 (100.00)	7 (87.50)	
Positive	2 (3.85)	4 (18.18)		0	1 (12.50)	
LVSI			0.143			0.320
Negative	42 (80.77)	14 (63.64)		21 (84.00)	5 (62.50)	
Positive	10 (19.23)	8 (36.36)		4 (16.00)	3 (37.50)	

Data presented as mean ± standard deviation. LVSI, lymph vascular space invasion; FIGO, International Federation of Gynecology and Obstetrics.

Table II. Univariate analysis of clinical characteristics.

Variable	Odds ratio	95% confidence interval	P-value
Age	0.986	0.979-0.993	0.002
Family history	0.500	0.120-2.077	0.423
Myometrial infiltration	0.636	0.287-1.409	0.350
FIGO stage	1.167	0.467-2.912	0.782
Lymph node status	2.000	0.481-8.314	0.423
LVSI	0.800	0.367-1.745	0.638

LVSI, lymph vascular space invasion; FIGO, International Federation of Gynecology and Obstetrics.

Validation of the model. Receiver operating characteristic curves were used to differentiate the diagnostic efficacy of the intratumoral and peritumoral models in distinguishing low-grade from high-grade EC. The AUC, accuracy, sensitivity and specificity were calculated. In addition, the Hosmer-Lemeshow (H-L) test and calibration curves were employed to assess model calibration.

Statistical analysis. Data analysis was performed using Python (version 3.7.12; https://python.hzjikj.cn/) and SPSS (version 26.0; IBM Corp.). The Shapiro-Wilk test was used to assess normality. Continuous variables following normal distribution are presented as mean ± standard deviation. Differences between low-grade and high-grade groups were compared using an unpaired Student's t-test, Fisher's exact test, Mann-Whitney U-test or χ^2 test. Univariate analysis assessed the association between clinical characteristics and tumor grade. P<0.05 was considered to indicate a statistically significant difference.

Results

Clinical characteristics. The training cohort consisted of 74 patients with a mean age of 56.42±10.17 years, including 52 patients in the low-grade group and 22 patients in the high-grade group. The test cohort included 33 patients, with 25 in the low-grade group and 8 in the high-grade group; the mean age was 56.06±11.75 years. No significant differences were noted in the other clinical characteristics between the two cohorts, except for the FIGO stage in the training cohort between the low- and high-grade groups (P=0.049), as detailed

Table III. Radiomic features in RT, RT-1, RT-2 and RT-3.

Category	Radiomic features
RT (n=7)	Intra original shape Sphericity, intra original shape Flatness, intra log sigma 20 mm 3D firstorder Kurtosis, intra log sigma 30 mm 3D firstorder Kurtosis, intra wavelet LLH glcm Idn, intra log sigma 5 0 mm 3D firstorder Skewness, intra log sigma 5 0 mm 3D glcm lmc2.1
RT-1 (n=3)	Peri original shape Flatness, peri wavelet LHH glszm LargeAreaHighGray LevelEmphasis, peri log sigma 2 0 mm 3D ngtdm Strength
RT-2 (n=4)	Peri original shape Flatness, peri wavelet HHL glszm LargeAreaHighGray LevelEmphasis, peri wavelet HLH glcm ClusterShade, peri wavelet LHH glszm SizeZoneNonUniformit
RT-3 (n=10)	Peri original shape Flatness, peri original firstorder Kurtosis.1, peri wavelet HHL ngtdm Complexity.1, peri log sigma 5 0 mm 3D glcm Idn.1, peri log sigma 50 mm 3D glszm ZoneVariance.1, peri wavelet HLH glcm ClusterShade, peri wavelet HHH glcm Correlation.1, peri wavelet HHL glcm ClusterProminence.1, peri wavelet LHH firstorder Mean.1, peri log sigma 20 mm 3D glcm ClusterShade

RT, peritumoral region; glcm, grey-level co-occurrence matrix; glszm, grey-level size zone matrix; ngtdm, neighboring grey tone difference matrix.

in Table I. Age was found to have statistically significant differences in the univariate analysis (Table II).

Radiomics features selection and model building. A total of 2,394 radiomic features were extracted from RT, RT-1, RT-2 and RT-3 regions, respectively. Following analysis using a Mann-Whitney U test and Pearson correlation analysis, the numbers of features retained were 531, 593, 573 and 575 from RT, RT-1, RT-2 and RT-3, respectively. Using mRMR and LASSO analyses, 7, 3, 4 and 10 features were selected to establish logistic regression models for RT, RT-1, RT-2 and RT-3, respectively. The detailed feature names are shown in Table III. The LASSO parameter l was optimized using 10-fold cross-validation, resulting in values of 0.0450, 0.0687, 0.0791 and 0.0518, as shown in Fig. 3.

Comparison and validation of models. The diagnostic performance of the intratumoral and peritumoral models with several expansion distances in differentiating between the low-grade and high-grade groups is presented in Table IV. In the test cohort, the AUCs were 0.869 (95% CI, 0.590-1.000), 0.840 (95% CI, 0.677-1.000), 0.850 (95% CI, 0.716-0.984) and 0.875 (95% CI, 0.744-1.000), respectively, with RT-3 indicating the optimal performance. In the training cohort, the RT-3 model exhibited an AUC of 0.934 (95% CI, 0.875-0.994), with sensitivity of 86.4%, specificity of 84.6% and a H-L test P-value of 0.958. In the test cohort, the RT-3 model exhibited an AUC of 0.875 (95% CI, 0.744-1.000), with sensitivity of 75.0%, a specificity of 88.0% and an H-L test P-value of 0.646. These results are shown in Fig. 4 and summarized in Table IV.

Establishment and validation of a fusion model. The fusion of the features was performed from RT and RT-3 (RT+RT-3), following the Mann-Whitney test, Pearson correlation analysis, mRMR and LASSO analysis. A total of 12 features were selected for model construction. The fusion model (RT+RT-3) demonstrated superior diagnostic performance in differentiating low-grade from high-grade EC over the single model (RT, RT-1, RT-2 and RT-3). In the training cohort, the model exhibited an AUC of 0.955 (95% CI, 0.910-1.000), sensitivity of 86.4%, specificity of 88.5% and an H-L test P-value of 0.992. In the test cohort, the following parameters were calculated: AUC=0.885 (95% CI, 0.771-1.000), sensitivity of 87.5%, specificity of 80.0% and an H-L test P-value of 0.264. The calibration curves indicate optimal agreement between actual outcomes and model predictions in both cohorts. The results are shown in Fig. 4 and summarized in Table IV.

Discussion

In the present study, radiomic features were extracted from T2WI and early dynamic contrast-enhanced images to predict the pathological grade of EC. The intratumoral features achieved sensitivities of 81.8% and specificities of 76.9% in the training cohort, and 62.5 and 80.0% in the test cohort, respectively. Following comparison of peritumoral regions expanded with 1, 2 and 3 mm, the data indicated that the 3 mm peritumoral region exhibited superior diagnostic performance, with sensitivities and specificities of 86.4 and 84.6% in the training cohort, and 75.0 and 88.0% in the test cohort, respectively. This may be related to the different degrees of infiltration between low-grade and high-grade endometrial cancers. Because the infiltration range of high-grade EC could be larger than that of low-grade EC, the performance of the 3-mm peritumoral region model is better than those at 1 and 2 mm. This may be related to the increased aggressiveness of higher-grade tumors.

Traditional pathological grading of EC relies on assessment of histomorphology, which can be subjective due to sample variability and interobserver differences (4). Previous

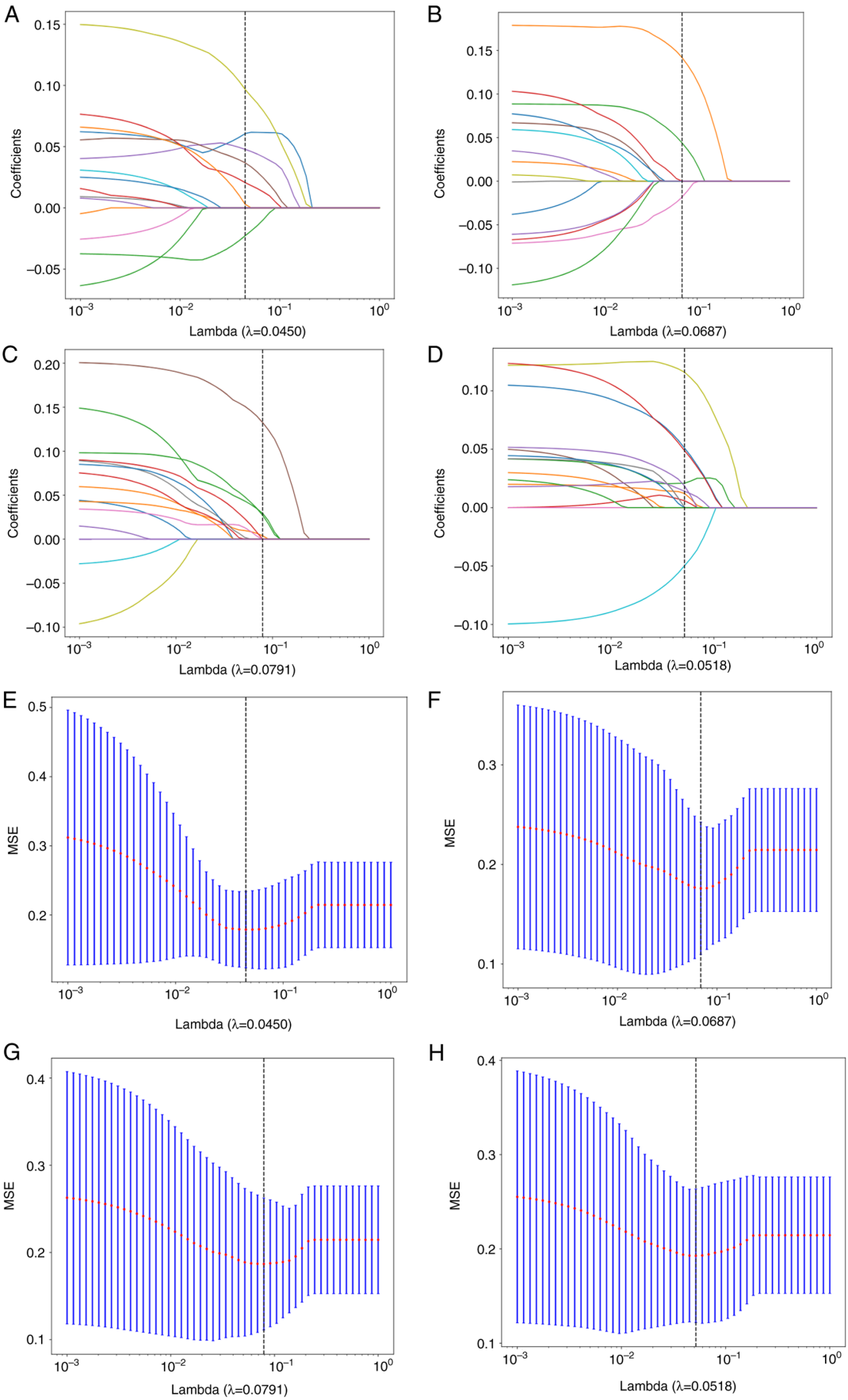

Figure 3. Radiomics feature selection using the LASSO regression method. LASSO coefficient profiles of the radiomics features in (A) RT, (B) RT-1, (C) RT-2 and (D) RT-3. A vertical line was drawn at the value selected using 10-fold cross-validation where optimal resulted non-zero coefficients (λ=0.0450, λ=0.0687, λ=0.0791 and λ=0.0518). The tuning parameter λ was selected using 10-fold cross-validation using the minimum criteria in the LASSO model in (E) RT, (F) RT-1, (G) RT-2 and (H) RT-3. The dashed line is the optimal λ. LASSO, least absolute shrinkage and selection operator; RT, peritumoral region; MSE, mean squared error.

Table IV. Comparison of the discriminative power of different models.

Model	Accuracy	AUC	95% CI	Sensitivity	Specificity	H-L test	Cohort
RT	0.784	0.879	0.797-0.962	0.818	0.769	0.892	Training
RT-1	0.730	0.884	0.756-0.931	0.864	0.673	0.349	Training
RT-2	0.824	0.872	0.786-0.957	0.636	0.904	0.607	Training
RT-3	0.851	0.934	0.875-0.994	0.864	0.846	0.958	Training
RT+RT-3	0.878	0.955	0.910-1.000	0.864	0.885	0.992	Training
RT	0.833	0.869	0.590-1.000	0.625	0.800	0.131	Testing
RT-1	0.788	0.840	0.677-1.000	0.625	0.840	0.490	Testing
RT-2	0.727	0.850	0.716-0.984	0.875	0.680	0.083	Testing
RT-3	0.848	0.875	0.744-1.000	0.750	0.880	0.646	Testing
RT+RT-3	0.818	0.885	0.771-1.000	0.875	0.800	0.264	Testing

RT, peritumoral region; CI, confidence interval; AUC, area under the curve; H-L, Hosmer-Lemeshow.

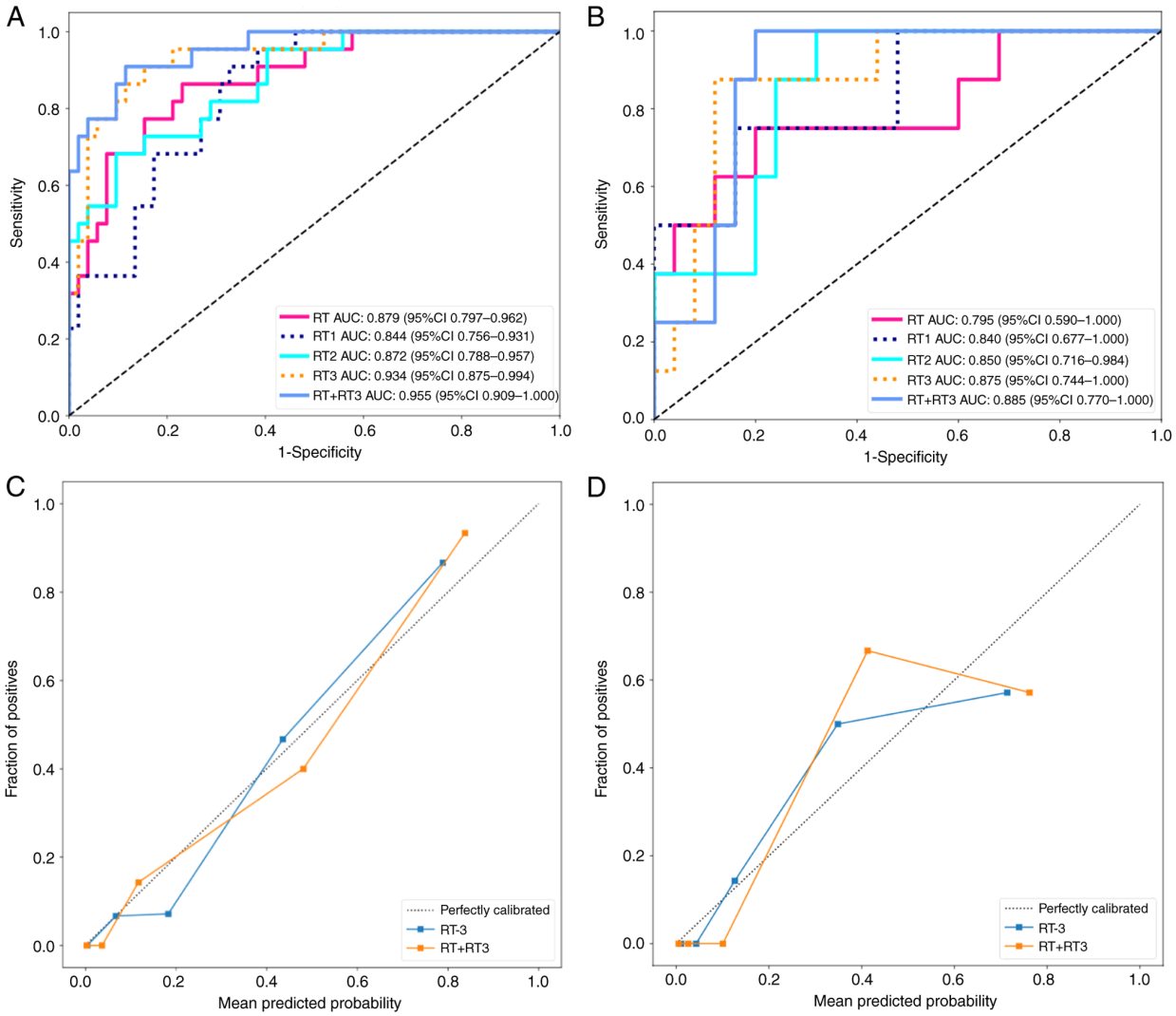

Figure 4. Receiver operating characteristic curves for the RT, RT-1, RT-2, RT-3 and RT+RT-3 models on the (A) training and (B) test cohorts. Calibration curves for the RT-3 and RT+RT-3 models on the (C) training and (D) test cohorts. RT, peritumoral region; AUC, area under the curve; CI, confidence interval.

studies have reported ~25% discordance between the preoperative biopsy-based pathological grade and the final surgical grade (26-28). Accurate pathological grading is vital for prognostic risk stratification in EC. Lower-grade tumors, with weaker invasive capabilities, may not extend peritumoral regions, resulting in different pathophysiological states between

high- and low-grade tumors (4). In the present study, the fusion of intratumoral and 3 mm peritumoral radiomic features demonstrated the optimal diagnostic performance for predicting pathological grade, with AUC values of 0.955 and 0.885 in the training and test cohorts, respectively. This provided new insights into the non-invasive EC grade assessment.

Moreover, in the present study, patients were grouped according to FIGO-recommended pathological grades (namely, G1/G2 as low-grade and G3 as high-grade) and the data indicated that the combined intratumoral and peritumoral radiomics model demonstrated strong predictive ability for EC grades, with sensitivity of 87.5% and specificity of 80.0% in the test cohort. The findings suggest that intratumoral and peritumoral radiomic data may provide value in revealing tumor biological characteristics, aiding clinicians in preoperative risk stratification. In addition, the present study revealed that EC clinicopathological features, such as family history, FIGO stage, myometrial invasion and lymph node metastasis were not significant in predicting low- or high-grade EC, possibly due to the small sample size of the study. Although the univariate analysis demonstrated a significant result for age in predicting endometrial cancer grade, the AUC values were reduced when age was incorporated into the multiple regression model. Therefore, future studies should investigate the integration of clinicopathological features in a larger sample size of ECs to enhance predictability.

The present study has the following limitations: i) The small sample size may limit the generalizability of the results; ii) the single-center study design requires external data for validation; iii) diffusion-weighted imaging was not included in the present study, which may lead to missing useful information; iv) the manual modification to ROIs for certain larger lesions may include additional pathologies or extrauterine tissues potentially impacting the outcomes; and v) due to the insufficient number of follow-up cases and changes in postoperative treatment, prognostic evaluation could not be performed in the present study. In future research, current research methods, combining Apparent Diffusion Coefficient and other MRI sequences will be included to evaluate the accuracy of radiomics indicators for the prognosis of EC.

In conclusion, the results of the present study demonstrate that integrating intratumoral and peritumoral MR radiomic features can aid prediction of EC grade. This non-invasive method has potential as a valuable tool for enhancing clinical management of EC, offering insights into patient treatment strategies without the requirement for invasive procedures.

Acknowledgements

The authors thank Mr. Liu Tao (Philips Healthcare, Beijing, China) for his technical assistance.

Funding

No funding was received.

Availability of data and materials

The data generated in the present study may be requested from the corresponding author.

Authors' contributions

JR, XL and ZS performed the data analysis and interpretation. TC and YZ collected and assembled the data. YY was involved in conception and design of the study. JR and YY confirm the authenticity of all the raw data. All authors read and approved the final version of the manuscript.

Ethics approval and consent to participate

The present study was approved by the Ethics Committees of the Beijing Shijitan Hospital [approval no. sjtkyll-lx-2020(3)]. Written informed consent for participation was obtained from patients and/or their legal guardians.

Patient consent for publication

Written consent for publication was obtained from patients and/or their legal guardians.

Competing interests

The authors declare that they have no competing interests.

References

1. Siegel RL, Miller KD, Fuchs HE and Jemal A: Cancer statistics, 2021. CA Cancer J Clin 71: 7-33, 2021.
2. Siegel RL, Giaquinto AN and Jemal A: Cancer statistics, 2024. CA Cancer J Clin 74: 12-49, 2024.
3. Clarke MA, Devesa SS, Harvey SV and Wentzensen N: Hysterectomy-corrected uterine corpus cancer incidence trends and differences in relative survival reveal racial disparities and rising rates of nonendometrioid cancers. J Clin Oncol 37: 1895-1908, 2019.
4. Concin N, Matias-Guiu X, Vergote I, Cibula D, Mirza MR, Marnitz S, Ledermann J, Bosse T, Chargari C, Fagotti A, *et al*: ESGO/ESTRO/ESP guidelines for the management of patients with endometrial carcinoma. Int J Gynecol Cancer 31: 12-39, 2021.
5. National Comprehensive Cancer Network: NCCN Clinical Practice Guidelines in Oncology (NCCN Guidelines): Uterine Neoplasms (Version1.2020) [EB/QL]. [2020-03-06]. Available from: https://www.nccn.org/pro-fessionals/physician_gls/pdf/uterine.pdf.
6. Satta S, Dolciami M, Celli V, Di Stadio F, Perniola G, Palaia I, Pernazza A, Della Rocca C, Rizzo S, Catalano C, *et al*: Quantitative diffusion and perfusion MRI in the evaluation of endometrial cancer: Validation with histopathological parameters. Br J Radiol 94: 20210054, 2021.
7. Lin G, Huang YT, Chao A, Ng KK, Yang LY, Ng SH and Lai CH: Influence of menopausal status on diagnostic accuracy of myometrial invasion in endometrial cancer: Diffusion-weighted and dynamic Contrast-enhanced MRI at 3 T. Clin Radiol 70: 1260-1268, 2015.
8. Zheng L, Zheng S, Yuan X, Wang X, Zhang Z and Zhang G: Comparison of dynamic contrast-enhanced magnetic resonance imaging with T2-weighted imaging for preoperative staging of early endometrial carcinoma. Onco Targets Ther 8: 1743-1751, 2015.
9. Keles DK, Evrimler S, Merd N and Erdemoglu E: Endometrial cancer: The role of MRI quantitative assessment in preoperative staging and risk stratification. Acta Radiol 63: 1126-1133, 2022.
10. Wang T, She Y, Yang Y, Liu X, Chen S, Zhong Y, Deng J, Zhao M, Sun X, Xie D and Chen C: Radiomics for survival risk stratification of clinical and pathologic stage IA Pure-solid Non-small cell lung cancer. Radiology 302: 425-434, 2022.
11. Hectors SJ, Lewis S, Besa C, King MJ, Said D, Putra J, Ward S, Higashi T, Thung S, Yao S, *et al*: MRI radiomics features predict immuno-oncological characteristics of hepatocellular carcinoma. Eur Radiol 30: 3759-3769, 2020.

12. Yang H, Yan S, Li J, Zheng X, Yao Q, Duan S, Zhu J, Li C and Qin J: Prediction of acute versus chronic osteoporotic vertebral fracture using radiomics-clinical model on CT. Eur J Radiol 149: 110197, 2022.
13. Dou G, Shan D, Wang K, Wang X, Liu Z, Zhang W, Li D, He B, Jing J, Wang S, *et al*: Integrating coronary plaque information from CCTA by ML Predicts MACE in patients with suspected CAD. J Pers Med 12: 596, 2022.
14. Pei Q, Yi X, Chen C, Pang P, Fu Y, Lei G, Chen C, Tan F, Gong G, Li Q, *et al*: Pre-treatment CT-based radiomics nomogram for predicting microsatellite instability status in colorectal cancer. Eur Radiol 32: 714-724, 2022.
15. Wan S, Zhou T, Che R, Li Y, Peng J, Wu Y, Gu S, Cheng J and Hua X: CT-based machine learning radiomics predicts CCR5 expression level and survival in ovarian cancer. J Ovarian Res 16: 1, 2023.
16. Kasius JC, Pijnenborg JMA, Lindemann K, Forsse D, van Zwol J, Kristensen GB, Krakstad C, Werner HMJ and Amant F: Risk stratification of endometrial cancer patients: FIGO stage, biomarkers and molecular classification. Cancers (Basel) 13: 5848, 2021.
17. Wang Y, Bi Q, Deng Y, Yang Z, Song Y, Wu Y and Wu K: Development and validation of an MRI-based radiomics nomogram for assessing deep myometrial invasion in early stage endometrial adenocarcinoma. Acad Radiol 30: 668-679, 2023.
18. Chen J, Wang X, Lv H, Zhang W, Tian Y, Song L and Wang Z: Development and external validation of a clinical-radiomics nomogram for preoperative prediction of LVSI status in patients with endometrial carcinoma. J Cancer Res Clin Oncol 149: 13943-13953, 2023.
19. Wang JJ, Zhang XH, Guo XH, Ying Y, Wang X, Luan ZH, Lv WQ and Wang PF: Prediction of lymphovascular space invision in endometrial cancer based on Multi-parameter MRI radiomics model. Curr Med Imaging 20: e15734056266366, 2024.
20. Bonatti M, Pedrinolla B, Cybulski AJ, Lombardo F, Negri G, Messini S, Tagliaferri T, Manfredi R and Bonatti G: Prediction of histological grade of endometrial cancer by means of MRI. Eur J Radiol 103: 44-50, 2018.
21. Nougaret S, Reinhold C, Alsharif SS, Addley H, Arceneau J, Molinari N, Guiu B and Sala E: Endometrial cancer: Combined MR volumetry and diffusion-weighted imaging for assessment of myometrial and lymphovascular invasion and tumor grade. Radiology 276: 797-808, 2015.
22. Yue X, He X, He S, Wu J, Fan W, Zhang H and Wang C. Multiparametric magnetic resonance imaging-based radiomics nomogram for predicting tumor grade in endometrial cancer. Front Oncol 13: 1081134, 2023.
23. Zheng T, Yang L, Du J, Dong Y, Wu S, Shi Q, Wang X and Liu L: Combination analysis of a Radiomics-based predictive model with clinical indicators for the preoperative assessment of histological grade in endometrial carcinoma. Front Oncol 11: 582495, 2021.
24. Soslow RA, Tornos C, Park KJ, Malpica A, Matias-Guiu X, Oliva E, Parkash V, Carlson J, McCluggage WG and Gilks CB: Endometrial carcinoma diagnosis: Use of FIGO grading and genomic subcategories in clinical practice: Recommendations of the international society of gynecological pathologists. Int J Gynecol Pathol 38 (Suppl 1): S64-S74, 2019.
25. Cui T, Shi F, Gu B, Jin Y, Guo J, Zhang C, Ren J and Yue Y: Peritumoral enhancement for the evaluation of myometrial invasion in Low-risk endometrial carcinoma on dynamic Contrast-enhanced MRI. Front Oncol 11: 793709, 2022.
26. Kurman RJ, Lora HE and Ronnett BM (eds): Blaustein's Pathology of the Female Genital Tract. 6th edition. Springer, London, 2011.
27. Batista TP, Cavalcanti CL, Tejo AA and Bezerra AL: Accuracy of preoperative endometrial sampling diagnosis for predicting the final pathology grading in uterine endometrioid carcinoma. Eur J Surg Oncol 42: 1367-1371, 2016.
28. van Hanegem N, Prins MM, Bongers MY, Opmeer BC, Sahota DS, Mol BW and Timmermans A: The accuracy of endometrial sampling in women with postmenopausal bleeding: A systematic review and meta-analysis. Eur J Obstet Gynecol Reprod Biol 197: 147-155, 2016.